Extension of droplet/aerosol heat transfer model coupling Lagrangian approach in containment atmosphere under severe accident

Fangnian Wang, Jianjun Xiao *, Thomas Jordan

Institute of Thermal Energy Technology and Safety (ITES), Karlsruhe Institute of Technology (KIT), Germany

ARTICLE INFO

Keywords:
Spray droplets
Aerosol
Heat transfer model
Condensation and evaporation
Lagrangian approach
Severe accident

ABSTRACT

Spray droplet dynamics are expected to significantly affect steam condensation, droplet evaporation, and global gas mixing in the containment atmosphere. During severe accidents, droplets may evaporate under high gas temperatures (>200 °C) such as hydrogen fire radiation, and water-soluble aerosols such as CsI and CsHO may dissolve in droplets. An extension of the droplet heat transfer model was conducted to account for these conditions and coupled with a Lagrangian approach for droplet tracking. The approach was comprehensively validated through single droplet experiments, demonstrating the feasibility of this new approach. Analyses of the effects of high atmosphere temperature, droplet curvature, and aerosol solute indicate that, 1) High gas temperature significantly reduces heat transfer, with the effect increasing at higher gas temperatures; 2) Droplet curvature enhances droplet evaporation, but this effect is limited to tiny droplets (<100 nm) compared to other effects; 3) The solute effect significantly impacts small droplet evaporation and dry aerosol growth, dominating the final equilibrium droplet diameter. The extended droplet/aerosol heat transfer model fills a gap in the knowledge of containment spray under severe accidents. A feasible way to approximate the minimum spray droplet size in the heat transfer model is to truncate or initialize the small droplet by the equilibrium diameter.

1. Introduction

Heat and mass transfer between spray droplets and the atmosphere is a classical scenario that is very common in industrial applications, such as raindrops on airfoils, liquid fuel spray in combustion engines, nuclear containment cooling, and so on (Amani and Nobari, 2013; Babić et al., 2009; Wang et al., 2021; Wu and Cao, 2015). During a loss-of-coolant accident at a nuclear power plant (NPP), steam is released from breaks or valves, and hydrogen can subsequently be generated by cladding oxidation, which can combust and explode in the containment vessel (IAEA, 2011). A spray system is an emergency containment cooling strategy designed to depressurize the atmosphere, remove heat from the atmosphere, mix the hydrogen, and wash out airborne radioactive aerosols inside the containment during the accident (van Sebille et al., 2018; Wang and Cheng, 2020). Spray droplet dynamics are expected to have significant effects on steam condensation and global gas mixing in the containment atmosphere. Therefore, spray droplet dynamics are of noticeable importance when evaluating the effectiveness of the containment spray system in an NPP.

Numerous investigations have been carried out on the heat and mass transfer of spray droplets in the atmosphere, both experimentally and numerically, over the past few decades. Early spray experiments were conducted in large-scale facilities, such as CSE (751 m3), NUPEC (1300 m3), and CVTR (6500 m3) (OECD, 1999). In the last 20 years, experiments on spray droplets in vessels conducted in small/intermediate-scale facilities include TOSQAN (7 m3), THAI (60 m3), MISTRA (98 m3), and PANDA (515 m3) (Gupta et al., 2017; Malet et al., 2011; Malet et al., 2011; Oecd, 2012), which have comprehensively investigated the influence of spray droplets on atmospheric behavior. In the field of nuclear engineering, most experiments have investigated droplet behavior in containment vessels generated via one or multiple spray nozzles. The data are not suitable for validating the heat transfer of a single droplet. The CARAIDAS experiment focused on the heat and mass transfer of a single droplet in the atmosphere (Malet et al., 2011), which was a separate-effect experiment investigating the motion and condensation/evaporation of a single droplet. There are very few experiments with single droplets under thermal–hydraulic containment conditions. Supplementary experiments for extending and validating heat transfer models include evaporation or condensation experiments of single droplets in air (Ranz and Marshall, 1952) and under the temperature of gas from fire/fuel combustion (Yuen and Chen, 1978).

* Corresponding author.
E-mail addresses: fangnian.wang@kit.edu (F. Wang), jianjun.xiao@kit.edu (J. Xiao), thomas.jordan@kit.edu (T. Jordan).

Nomenclature

A	particle/droplet projected area, m^2
A_p	particle/droplet surface area, m^2
B_m	mass Spalding number
B_T	heat Spalding number
C_d	drag force coefficient
c	constant
c_p	water specific heat capacity, J/(kg·K)
$c_p, c_{p,v}, c_{p,g}$	water, vapor, gas specific heat capacity, J/(kg·K)
D	binary diffusion coefficient, m^2/s
d	particle/droplet diameter, m
$\boldsymbol{F}_D$	drag force vector, N
$\boldsymbol{F}_b$	buoyancy force vector, N
$\boldsymbol{G}_p$	particle/droplet gravity, N
$\mathbf{g}$	gravity acceleration, m/s^2
h	heat transfer coefficient, $W/(m^2{\cdot}^\circ C)$
I_s	Van't Hoff factor
k_c	mass transfer coefficient, $kg/(m^2{\cdot}s)$
L_{fg}	latent heat for the droplet evaporation/condensation, J/kg
M_w	water molecular weight, 0.01802 kg/mol
M_s	salute molecular weight, e.g. CsI, 0.25981 kg/mol
Nu	Nusselt number
n_s	moles of total dissolved solute, mol
n_w	moles of water, mol
Pr	Prandtl number
p	pressure, Pa
$P_{v,surf}$	water vapor pressure on surface, Pa
P_{sat}	saturated water vapor pressure, Pa
R	molar gas constant, 8.314 J/(K·mol)
Re_p	particle/droplet Reynolds number
r	water droplet radius, m
Sc	Schmidt number
Sh	Sherwood number
T	temperature, K
T_{surf}	particle surface temperature, K
T_∞	gas temperature in the bulk, K
T_p	particle/droplet temperature, K
t	time, s
U_t	droplet terminal velocity
$\boldsymbol{u}_g$	gas velocity vector, m/s
$\overline{\boldsymbol{u}}_g$	gas time-averaged velocity, m/s
$\boldsymbol{u}'_g$	gas velocity fluctuation, m/s
$\boldsymbol{u}_p$	particle/droplet velocity vector, m/s
y	vapor mass fraction
y_{surf}	vapor mass fraction on surface
α	thermal diffusivity/particles volume fraction in gas cell, m^2/s, -
λ_g	thermal conductivity, W/(m·K)
ζ	normally distributed numbers
κ	turbulent kinetic energy, m^2/s^2
μ	dynamic viscosity, Pa·s
ρ	density, kg/m^3
ρ_g	gas density, kg/m^3
ρ_p/ρ_w	particle/droplet density, kg/m^3
ρ_s	solution density, kg/m^3
$\rho_{h_2o,\infty}$	steam density in the bulk, kg/m^3
σ_w	water surface tension, N/m
τ_p	particle response time, s

Numerical analyses of spray effects on NPP containment atmosphere have been performed using Lumped-Parameter (LP) and Computational Fluid Dynamics (CFD) codes. LP codes, such as MELCOR, COCOSYS, ASTEC, etc., describe a nuclear containment as a network of control volumes/zones connected with flow paths/junctions, which simulate a long physical time accident scenario quickly but cannot provide the local field details. In contrast, CFD codes capture the local field (e.g. ANSYS/CFX, OpenFOAM, GASFLOW, etc.) and are recently preferred for investigating the containment spray phenomena. The authors prefer to adopt the modelling approach of using the Eulerian method for the continuous gas phase and Lagrangian method for the dispersed droplet phase. The use of the Lagrangian approach has gained significant importance in recent decades due to various reasons, including advancements in computer power and the development of stochastic modeling to account for the turbulence effect on droplet trajectories. The literature related to the importance of the Lagrangian approach in different research fields shows that it has been extensively used in various applications, including atmospheric studies (e.g., tracking of atmospheric particles and pollutants (Tinarelli et al., 2012), oceanography (e.g., modeling of ocean circulation and plankton distribution (van Sebille et al., 2018), and fluid mechanics (e.g., simulating turbulent flows and particle-laden flows (Kuerten, 2016).

In the nuclear field, Babić et al. (Babić et al., 2009) presented a two-way interaction approach in the CFD code ANSYS/CFX4.4 to solve droplet transport using the Lagrangian droplet-tracking model via user-defined subroutines. Whang et al. (Whang et al., 2021) also implemented the Eulerian (carrier gas) – Lagrangian (dispersed droplets) approach in OpenFOAM to calculate this two-phase phenomenon and analyze the effects of buoyancy and droplet size. The mass and momentum interaction between the two phases were considered, but heat and mass transfer were neglected. Ding et al. (Ding et al., 2017) developed a similar approach and implemented it into the GASFLOW code, where heat and mass transfer between water droplets and gas were considered. Although Ding et al. mentioned droplet-wall interaction in their simulations, they did not describe the model or discuss the effects on the results. Mimouni et al. (Mimouni et al., 2010) proposed a droplet-wall interaction model dedicated to the evaporation of droplets attached to a heated wall and surrounded by hot gas. In these literatures, the two-way coupling approach usually assumes that droplet-to-droplet interactions (droplet fragmentation and coalescence) are neglected due to the complexity of spray droplet collision (Foissac et al., 2011; Foissac et al., 2013; Rabe et al., 2010).

However, none of the heat transfer models used in CFD modelling (Babić et al., 2009; Ding et al., 2017; Mimouni et al., 2010; Whang et al., 2021) consider the particularities of droplet heat transfer in severe accident conditions, such as the effects of high gas temperatures (>200 °C) and aerosol solutes. The acquired knowledge of heat transfer of a single droplet is essential to understand and predict the performance of water sprays. However, most of the work done in the past has been concentrated in environmental temperatures from 20 °C to 150 °C. During severe accidents, the containment temperature could be very high due to hydrogen fires. From previous works (Renksizbulut and Yuen, 1983; Renksizbulut et al., 1991; Yuen and Chen, 1976; Yuen and Chen, 1978; Zhifu et al., 2013), a clear picture of the effect of evaporation on droplet heat transfer emerges. The mass flux from evaporation dynamically affects the flow field surrounding the droplet. Meanwhile, evaporation causes large temperature gradients and changes the chemical composition (e.g., dissolved aerosols). These effects could significantly alter the heat and mass transfer processes. Furthermore, during severe accidents, the evaporating droplets and aerosol particles (hygroscopic growth) could be small <100 nm. The curvature effect should be considered when calculating the heat transfer (Bowley, 2021), as the greater the droplet curvature, the greater the chance that water molecules on the surface can escape, thus increasing the evaporation rate. On the

contrary, if aerosol particles that are soluble in water, such as Cesium iodide (CsI) and Cesium hydroxide (CsOH), are present in the atmosphere, they can dissolve in water droplets. The concentration of solute (CsI, CsOH, etc.) prevents water molecules from escaping from the droplet surface. Adding more solute to the solution makes it more difficult for water molecules to escape (Bowley, 2021). These effects are often considered in aerosol growth in the atmosphere (Köhler, 1936) (Pruppacher and Klett, 1980), including the radioactive aerosol growth in nuclear containment (Li et al., 2020; Mishra et al., 2019), but are rarely seen in the spray droplet heat transfer model.

In a short summary, there is a tendency to adopt the Lagrangian droplet-tracking approach to model the spray droplets in the atmosphere. However, advanced considerations on droplet heat and mass transfer models are worthy of implementation in a newly developed approach, such as the effects of high gas temperature, droplet curvature, and the aerosol solute. The above aspects are taken into account in the extension of the droplet heat transfer model. The behaviors of a single droplet in evaporation and condensation atmosphere conditions are investigated with respect to each new consideration.

2. Lagrangian approach

2.1. Universal droplet-tracking model

The Lagrangian droplet-tracking method describes the movement of the spray droplets as the spatially dispersed phase (Ding et al., 2017). The dispersed phase is considered to be in the form of discrete single-component spherical liquid droplets (Babić et al., 2009). Momentum transfer between phases is a function of the drag force. The energy and mass exchange between phases are assumed to occur through convective heat transfer and the resulting condensation/evaporation. For two-way coupling, the generic Lagrangian equations describing the velocity ($\boldsymbol{u}_p$), mass (m_p), and temperature (T_p) of one simulated single particle/droplet represent a particular group (particle cloud).

The droplet velocity $\boldsymbol{u}_p$ is determined by the sum of the forces acting on the particle, namely the drag force $\boldsymbol{F}_D$, gravity $\boldsymbol{G}_p$, and buoyancy force $\boldsymbol{F}_b$:

$$m_p\frac{d\boldsymbol{u}_p}{dt} = \boldsymbol{F}_D + \boldsymbol{G}_p + \boldsymbol{F}_b \tag{1}$$

The gravity force and buoyancy force are combined as:

$$\boldsymbol{G}_p + \boldsymbol{F}_b = \frac{\pi}{6}d^3\mathbf{g}(\rho_p \quad \rho_g) \tag{2}$$

The shape of the liquid droplet is assumed to be spherical, so the drag force can be calculated:

$$\boldsymbol{F}_D = \frac{1}{2}C_d\rho_g A|\boldsymbol{u}_g \quad \boldsymbol{u}_p|(\boldsymbol{u}_g \quad \boldsymbol{u}_p) \tag{3}$$

where A is the droplet projected area on the velocity direction,$A = \frac{1}{4}\pi d^2$. The subscripts g and p denote gas and particle, respectively. ρ_g is the gas density. C_d is the drag force coefficient depending on particle Reynolds number (Putnam, 1961):

$$\mathrm{Re}_p = \frac{\rho_g|\boldsymbol{u}_g \quad \boldsymbol{u}_p|}{\mu_g} \tag{4}$$

$$C_d = \begin{cases} \dfrac{24}{\mathrm{Re}_p} + 4.5\mathrm{Re}_p < 5 \\ \dfrac{24}{\mathrm{Re}_p}\left(1 + \dfrac{1}{6}\mathrm{Re}_p^{2/3}\right) 5 < \mathrm{Re}_p \le 1000 \\ 0.44\mathrm{Re}_p > 1000 \end{cases} \tag{5}$$

For perfect laminar flow $Re_p < 5$, Oseen (Oseen, 1910) extended the coefficient from Stokes' law by taking the inertia terms in the Navier-Stokes equations partly into account. For turbulent wake flow $Re_p > 1000$; the drag coefficient remains approximately constant 0.44 (the so-called Newton's law for the terminal velocity). For the flow between the above two regimes $5 < Re_p \le 1000$, the coefficient is usually given by an empirical correlation, e.g. Schiller and Naumann (Schiller and Naumann, 1935) correlation currently.

The gas velocity in the definition of particle Reynolds number Re_p should take into account the turbulence effects of gas, i.e.

$$\boldsymbol{u}_g = \overline{\boldsymbol{u}}_g + \boldsymbol{u}_g' \tag{6}$$

where $\overline{\boldsymbol{u}}_g$ are the gas and particle time-averaged velocities. $\boldsymbol{u}_g'$ is the velocity fluctuations of gas. The turbulent dispersion can be obtained by the discrete random walk model, namely the velocity fluctuation follows the Gaussian distribution random presumptively.

$$\boldsymbol{u}_g' = \zeta\sqrt{\frac{2\kappa}{3}} \tag{7}$$

where ζ is normally distributed numbers, and κ is the turbulence kinetic energy of gas.

The droplet heat and mass transfer model is applied to estimate the evaporation/condensation rate:

$$\frac{dm_p}{dt} = \quad k_c A_p \rho_{g,\infty} ln(1 + B_m) \tag{8}$$

$$m_p c_p \frac{dT_p}{dt} = hA_p(T_\infty \quad T_p) + \frac{dm_p}{dt}L_{fg} \tag{9}$$

where $B_m = \frac{y_{h_2o,sat} \quad y_{h_2o,\infty}}{1 \quad y_{h_2o,sat}}$ is the mass Spalding number, $y_{h_2o,sat}$ and $y_{h_2o,\infty}$ are the vapor mass fraction at droplet surface (saturated) and in the bulk gas, respectively. L_{fg} is the latent heat for the droplet evaporation/condensation, and $A_p = \pi d^2$ is the surface area of the droplet. h and k_c are the heat and mass transfer coefficients, respectively, which are determined by the Nusselt number $\mathrm{Nu} = \frac{hd}{\lambda_g}$ and Sherwood number $\mathrm{Sh} = \frac{k_c d}{D}$. D is the binary diffusion coefficient. These two dimensionless numbers are calculated by the widely used Ranz and Marshall correlations (Ranz and Marshall, 1952):

$$\mathrm{Nu} = 2 + 0.552\mathrm{Re}_p^{1/2}\mathrm{Pr}^{1/3} \tag{10}$$

$$\mathrm{Sh} = 2 + 0.552\mathrm{Re}_p^{1/2}\mathrm{Sc}^{1/3} \tag{11}$$

where $Pr = \frac{\mu_g C_p}{\lambda_g}$ and $Sc = \frac{\mu_g}{\rho_g D}$ are the gas Prandtl number and Schmidt number, respectively. The "1/3 rule" is used to estimate the droplet surface temperature T_{surf}, and the vapor mass fraction y_{surf}:

$$T_{surf} = T_p + \frac{1}{3}(T_\infty \quad T_p) \tag{12}$$

$$y_{surf} = y_{h_2o,p} + \frac{1}{3}(y_{h_2o,\infty} \quad y_{h_2o,p}) \tag{13}$$

The vapor mass fraction at the droplet surface $y_{h_2o,p}(T_p)$ is obtained when the droplet temperature is given. Note that Ref. (Yuen and Chen, 1976) recommended using y_{surf} for calculating the thermal properties in the thin gas layer around the droplet surface. The Lagrangian droplet-tracking equations (mass, momentum, energy) are solved via the implicit algorithm.

2.2. Extension of droplet heat transfer model

2.2.1. Effect of high gas temperature

During severe accidents, the spray droplets may be surrounded by a high-temperature atmosphere (>200 °C), including a hydrogen fire. A high rate of phase change is expected, and special attention should be paid to the effect of fast heat and mass transfer. This is because the steam

concentration near the droplet surface is significantly different from the bulk concentration. To account for the fast phase change effect, the Ranz and Marshall correlations should be corrected. Renksizbulut et al. (Renksizbulut and Yuen, 1983; Renksizbulut et al., 1991) measured heat transfer rates to simulated and freely suspended water droplets in an atmospheric hot air tunnel with Reynolds numbers ranging from 25 to 2000. They found that the experimental data can be correlated by introducing a factor that multiplies the Ranz and Marshall correlations, indicating that evaporation reduces heat transfer rates directly by a factor of $(1+B_T)^{-0.7}$ at higher temperatures. Zhifu et al. (Zhifu et al., 2013) summarized various methods for modeling heat and mass transfer between the droplet (fuel) and gas phases (in the burning chamber). They tested the validity of various models by comparing model predictions to three sets of experiments with small, intermediate, and large evaporation rates. They found that all models perform nearly identically for cases with low evaporation rates, but significant deviations among model predictions emerge when the evaporation rate increases. Finally, they propose a uniform formulation based on Ranz and Marshall correlations with a correction factor as follows:

$$Nu^* = (1+B_T)^{-2/3}\left(2+0.552Re_p^{1/2}Pr^{1/3}\right) \tag{14}$$

$$Sh^* = (1+B_m)^{-2/3}\left(2+0.552Re_p^{1/2}Sc^{1/3}\right) \tag{15}$$

where B_T and B_m are the heat and mass Spalding numbers (Spalding, 1953). B_T is a function of B_m(Abramzon and Sirignano, 1989);

$$B_T = (1+B_m)^{\left(\frac{c_{p,v}}{c_{p,g}}\right)\left(\frac{Sh^*}{Nu^*}\right)\frac{1}{Le}} \quad 1 \approx (1+B_m)^{\left(\frac{\rho_g D c_{p,v}}{\lambda_g}\right)} \quad 1 \tag{16}$$

where $c_{p,v}$ is vapor specific heat capacity, the Lewis number $Le = \frac{\lambda_g}{\rho_g D c_{p,g}}$. Note that the heat Spalding number B_T is obtained by the iteration of corrected Nu and Sh numbers, however, it can be approximated via assuming $\frac{Sh^*}{Nu^*} \approx 1$ (Strizhak et al., 2018).

Furthermore, the droplet diameter, as well as the droplet velocity, becomes small due to the evaporation. At low Reynolds number ($Re_p \leq 10$) of droplet, the Ranz and Marshall correlations (Ranz and Marshall, 1952) overestimate the transfer rate. As an alternative, the following correlations by Clift et al. (Clift et al., 1978) are recommended when $Re_p \leq 400$, which can be coupled in the correction for high temperature atmosphere.

$$Nu = 1 + \left(1+Re_pPr\right)^{1/3} max\left(1, Re_p^{0.077}\right) \tag{17}$$

$$Sh = 1 + \left(1+Re_pSc\right)^{1/3} max\left(1, Re_p^{0.077}\right) \tag{18}$$

2.2.2. Curvature (Kelvin) effect

During severe accidents, spray droplets and aerosol particles (undergoing hygroscopic growth) can be very tiny, with diameters smaller than 100 nm. For the heat and mass transfer of these small droplets, the curvature (Kelvin) effect should be considered for calculating the vapor partial pressure on the droplet surface (Bowley, 2021; Topping et al., 2005). This effect considers that the droplet size modifies the droplet surface tension. The surface tension force, a net inward attractive force, increases as the droplet diameter reduces. Therefore, there is a greater probability of a water molecule escaping from the liquid and entering the vapor phase as the diameter decreases. As the curvature increases, the surface water molecules can escape more easily. It takes less energy to remove a molecule from a curved surface than from a flat surface. As a result, the evaporation rate increases when the diameter decreases.

The Kelvin Equation corrects the vapor pressure on a curved droplet surface:

$$\frac{P_{v,surf}}{P_{sat}\left(T_{surf}\right)} = exp\left(\frac{4\sigma_w}{RT_{surf}n_w d}\right) = exp\left(\frac{4M_w\sigma_w}{RT_{surf}\rho_w d}\right) \tag{19}$$

where $P_{v,surf}$ is the equilibrium water vapor pressure over the droplet surface, $P_{sat}\left(T_{surf}\right)$ is the saturated vapor pressure over a flat surface, σ_w is the water surface tension, n_w is the number of moles of liquid water per unit volume, and R is the universal gas constant. Note the pronounced increase in vapor pressure for particles that have small radius (<100 nm). The Kelvin effect is important only for tiny droplets. As the droplet gets bigger enough (radius increases), the ratio $\frac{P_{v,surf}}{P_{sat}\left(T_{surf}\right)}$ approaches 1. Assuming that the σ_w and ρ_w vary little with temperature and the solute of aerosols (discussed later), the ratio can be approximated as $exp\left(\frac{6.6\times10^{-7}}{T_{surf}d}\right)$ (Pruppacher and Klett, 1980).

2.2.3. Solute effect (Raoult's Law)

During severe accidents, the containment atmosphere is not clean. There are types of soluble aerosol particles in the atmosphere, most of which are hydrophilic and water-soluble, such as cesium iodide (CsI), cesium hydroxide (CsOH), and other possible soluble dry aerosols (Foissac, 2011). They like water and dissolve in water droplets. The solutes of the radioactive chemical compounds (CsI, CsOH, etc.) could dissolve in the solvent spray water droplets. The molecules of the chemical compounds are distributed in the water (solvent), and therefore some solute molecules occupy surface sites and prevent water molecules from escaping. Adding more solute means that more surface sites would be occupied by solute molecules, and water vapor would have even less opportunity to break hydrogen bonds and escape the liquid. The real mechanism is more complicated due to the electrostatic interactions between water and solute molecules that cause an attraction between them, but the basic result is the same as the above explanation (Bowley, 2021).The vapor pressure over a solution can be quantified with Raoult's Law, which describes the solute effect (chemical activity) that tends to decrease vapor pressure over a solution droplet:

$$\frac{P_{v,surf}}{P_{sat}\left(T_{surf}\right)} = exp\left(\frac{I_s M_w \frac{m_s}{M_s}}{\frac{\pi d^3 \rho_s}{6} - m_s}\right) \approx exp\left(\frac{2n_s}{n_w}\right) \tag{20}$$

here, I_s is the number of ions generated by a solute molecule dissociation, which is called the Van't Hoff factor and accounts for the splitting of the solutes into components when they dissolve. For example, CsI splits into two ions in solution, Cs + and I–, so in this case, $I_s = 2$. M_w and M_s are the molecular weights of pure water and solute, respectively. m_s is the mass of dissolved solute, and n_s is the moles of total dissolved solute in a wet particle. For the sufficiently dilute solution, assumptions are usually applied when calculating the chemical activity (Pruppacher and Klett, 1980). Since the droplet is very tiny, there is no significant temperature gradient between the droplet and atmosphere, $dT/dt \approx 0$ thus $T_\infty = T_{surf}$. The solute mass is much less than the water mass, $m_s \ll m_w$. Water density equals solution density, $\rho_w = \rho_s$. To calculate the Kelvin effect, the water surface tension equals the solution surface tension, $\sigma_w = \sigma_s$.

A combination of the two expressions, the Kelvin equation and Raoult's law, is often used to describe the vapor pressure change on the surface of a small water droplet with solute (Köhler, 1936; Pruppacher and Klett, 1980). The Kelvin term governs the increase in water vapor pressure over a curved surface, while the Raoult's law term describes the solute effect that tends to decrease vapor pressure over a solution droplet. The modified vapor pressure is used to correct the mass fraction of vapor and the B_m in the droplet heat and mass transfer model.

$$\frac{P_{v,surf}}{P_{sat}(T_{surf})} = exp\left(\frac{4\sigma_s}{RT_{surf}n_w d}\ \frac{I_s M_w \frac{m_s}{M_s}}{\frac{\pi d^3 \rho_s}{6}\ m_s}\right) \tag{21}$$

3. Model validation

3.1. Free-falling droplet without heat and mass transfer

To validate the Lagrangian droplet-tracking model implemented in the GASFLOW code, we investigated the velocity of a free-falling droplet without heat and mass transfer. We compared the terminal velocities of water droplets with various sizes falling in stagnant air, as measured by Gunn and Kinzer (Gunn and Kinzer, 1949), with the calculated results, which revealed a very small deviation (maximum discrepancy is 0.2%), as shown in Table 1. The air pressure was 1 atm, and the temperature was 20 °C. The air density (relative humidity 50%) was 1.198 kg/m3, and the density of the particle was 1.0 X 10^3 kg/m^3. The air dynamic viscosity was 1.795 X10^{-5} kg/(m·s). The particle diameter and constant drag coefficient, C_d, are listed in Table 1. The gravitational settling of a single particle was calculated by balancing the drag force. The terminal velocity is given by:

$$u_p(\infty) = \lim_{t\to\infty} U_t\left(\frac{1 - e^{-2gt/U_t}}{1 + e^{-2gt/U_t}}\right) = U_t = \sqrt{\frac{4\rho_p d\mathbf{g}}{3C_d\rho_g}} \tag{22}$$

Due to the tiny mass loading of the discrete phase, the effect of the discrete phase on the continuous phase is negligible. In principle, the calculation results of one-way and two-way coupling should be identical. One-way means the particle does not influence the flow. The two-way coupling results are the first glance on code verification. More validation details of the two-way momentum coupling in GASFLOW are presented in the companion paper (Wang et al., 2023). The calculations are compared with the theoretical solutions, as shown in Fig. 1. The particle velocity increases with time due to the gravity, and eventually reaches a constant terminal velocity. It seems that both the momentum predictions of one-way and two-way coupling have good agreements with the analytical solution. For more details, please refer to our previous work (Xiao et al., 2013).

3.2. Stagnant droplet evaporates in the dry air

Simulations were conducted to validate the heat and mass transfer model by studying the evaporation of a single, isolated droplet. The experiment by Ranz and Marshall (Ranz and Marshall, 1952) investigated the evaporation dynamics of a motionless droplet. In our numerical setup, a stagnant droplet with an initial diameter of 1.05 mm was placed in air with 0% relative humidity (dry air) and temperature of 25 °C. The droplet's initial temperature was 9 °C. The temperature difference between the droplet and bulk gas was so small that the thermal properties were assumed to be constant. The droplet's diameter was tracked as it evaporated in the surrounding environment, and the results were compared to experimental data. Fig. 2 shows the comparison between the simulation results, analytical solution, and experimental data, which reveal excellent agreement. The 'Python' legend refers to the predictions made by our in-house Python code, which solves the coupling mass and energy ordinary differential equations

Table 1
Comparison of the measured and analytical terminal velocity.

Case	d_p, cm	C_d	m_p, mg	Re_p	U_t, exp., cm/s	U_t, cal., cm/s
1	0.05	1.28	0.0655	68.7	206	206.4
2	0.10	0.671	0.524	269	403	403.2
3	0.20	0.517	4.190	866	649	649.6
4	0.30	0.503	14.140	1613	806	806.5
5	0.50	0.660	65.500	3033	909	909.1

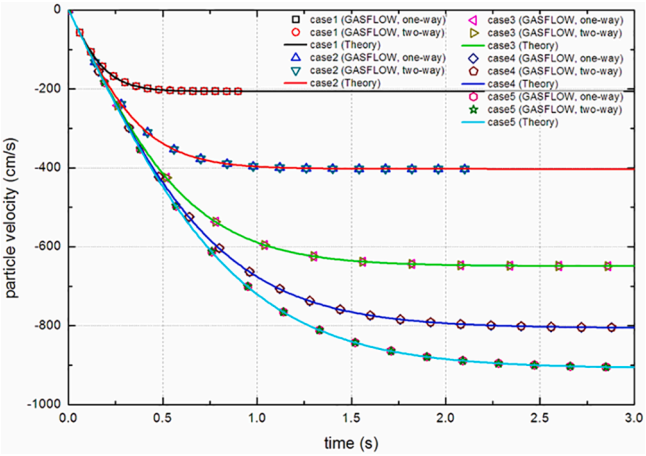

Fig. 1. Comparison of theoretical and calculated particle settling velocity.

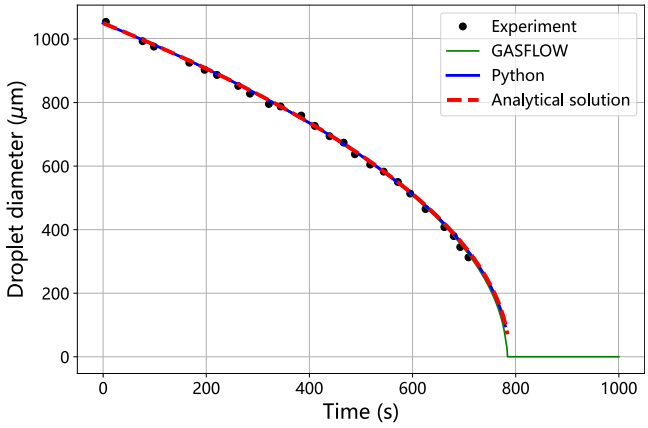

Fig. 2. Stagnant droplet evaporation in dry air.

using the SciPy library. The prediction of a stagnant droplet evaporating in dry air with Ranz and Marshall correlations shows good agreement with most of the experimental data.

The analytical solution is the droplet evaporation represented by the d^2- law, which states that the square of the droplet diameter varies linearly with time (Crowe et al.,). The d^2- law can be shown by application of the mass equation, which can be rewritten as:

$$\frac{dm_p}{dt} = \frac{d\left(\rho_p \frac{\pi}{6} d^3\right)}{dt} = h_m A_p \rho_{g,\infty} ln(1 + B_m) = Sh\pi D d\rho_{g,\infty} ln(1 + B_m) \tag{23}$$

$$d\frac{dd}{dt} = \frac{2Sh D\rho_{g,\infty}}{\rho_p} ln(1 + B_m) \tag{24}$$

Taking the right side as constant and integrating the equation yields:

$$d^2 = d_0^2 \quad c \bullet t \tag{25}$$

where the constant $c = \frac{4ShD\rho_{g,\infty}}{\rho_p} ln(1 + B_m)$. This mass equation form has been used extensively. Data for droplet evaporation have been frequently reported as a value for c. Obviously, c will not be a constant in a flow with changing freestream conditions, but for many situations the approximation may be adequate (Crowe et al., 2012). The lifetime $\frac{d_0^2}{c}$ of an evaporating droplet is obtained by setting $d = 0$.

In the Ranz and Marshall experiment, the droplet is stagnant, therefore, the evaporation occurs primarily due to the diffusional effect (i.e. Sh ≈ 2, see the Ranz and Marshall correlations in case of $Re_p = 0$). The temperature between the droplet and bulk gas is quite small, so that

the droplet temperature can be assumed having a slight change during the evaporation. The constant $c = 1.4 \times 10^{-9}$ m^2/s, which is obtained by using the initial droplet temperature 9 °C. The lifetime of this evaporating droplet $\frac{d_0^2}{c}$ is around 787.5 s.

3.3. Steam condensing and droplet evaporating in moist air

The mass, momentum, and heat transfers of a single droplet were investigated in the IRSN CARAIDAS facility (Malet et al., 2011; Plumecocq and Passalacqua, R., 2001). CARAIDAS experiments studied droplet evolution under typical post-accident atmospheric conditions. The cylindrical enclosure is 5 m high with a 0.6 m inner diameter. Homogeneous atmospheric conditions with gas temperatures ranging from 20 to 160 °C, absolute pressures ranging from 1 to 8 bar, and relative humidity ranging from 3 to 95% are prepared before droplet injection. The drop generator is located at the top of the vessel to maintain a constant temperature regardless of the vessel temperature. The generated water droplets have diameters ranging from 200 to 700 μm and temperatures ranging from 20 to 80 °C. After a droplet is injected into the vessel, its diameter is modified by steam condensation or/and droplet evaporation. The droplet diameter is optically measured at three elevations: at the top (droplet generator, z = 0 m), at z = 2.51 m, and at the bottom (z = 4.39 m). The specific test conditions with mean values are given in TABLE. 2: 'evaporation' and 'condensation' tests are named EVAP-i and COND-i, respectively. More details of the experiments can be found in Refs. (Malet et al., 2011; Plumecocq and Passalacqua, R., 2001).

Information on droplet velocity or droplet temperature is not available; thus, both are only subject to the code-to-code comparison. The code-experiment comparison is presented in Fig. 3 for the droplet sizes at the lowest location (Z = 4.39 m). The analytical solutions are obtained by the Python code, which solves the coupling mass, momentum, and energy ordinary differential equations of a single droplet. Thermal properties here are obtained via polynomial temperature functions. The comparison indicates that the predictions of droplet diameters are in good agreements with the experimental data. Note that the droplet in case EVAP24 evaporates completely.

Nevertheless, the main discrepancies are obtained in tests EVAP13, EVAP18, and EVAP21 (relative error < 20% in the current work). Similar results were demonstrated in the SARNET-2 activities, regardless of the results obtained via LP or CFD codes (Malet et al., 2011). Some predictions in SARNET-2 activities have quite large errors (e.g., evaporating completely in EVAP18 and having about a 70% relative error in EVAP21). It is worth to note that the heat and mass transfer correlations used in SARNET-2 activities are exactly the same as Ranz and Marshall correlations with a slight change of the constants. According to the boundary conditions of tests EVAP13, EVAP18, and EVAP21, some common points can be found: the relative humidity is low (3–15%), the temperature difference between the droplet and moist air is high (68.2–104.3 °C), indicating that more attentions should be paid to continuous evaporation.

Fig. 4 (a) and (b) present the evolutions of droplet diameter and temperature of tests COND7 and EVAP21. The results labeled CFX_IRSN are the predictions from IRSN using the CFD code ANSYS/CFX, which are extracted from Ref. (Malet et al., 2011). In test COND7, the droplet diameter increases firstly and decreases almost linearly later due to the condensation on the droplet and evaporation of the droplet successively. It can be seen that in test EVAP21 the differences between the calculations become higher as the droplet size decreases with evaporation. Generally, before the vertical displacement is 1 m from the injection point, the reached droplet equilibrium temperature is rather similar between all calculations. The relative difference between the equilibrium temperature obtained is lower than 5% (<10 °C). The developments of droplet velocity alone the vertical displacement are presented in Fig. 4 (c). The droplet velocity in COND10 is accelerated, while in EVAP13 it is decelerated to the terminal equilibrium velocity. The settling velocity of the droplet, with no longer evaporation or condensation, can be obtained theoretically via the balance between drag and gravity forces. The values presented in Fig. 4 (c) given by all calculations indicate that the bias is generally lower than 20%.

4. Analysis and discussion

4.1. Effect of high atmosphere temperature

The dimensionless heat transfer rate, Nusselt number, of liquid droplets' evaporation/condensation is function of Reynolds number and Prandtl number, as the Ranz and Marshall correlation and the extended correlation presented in Section 2. In nuclear containment spray, the range of Reynolds numbers of interest for heat and mass transfer of liquid droplets is generally below 2000. Ranz and Marshall represents the best correlation in most codes (ANSYS/FLUENT, ANSYS/CFX, etc.) for evaporating liquid droplets and steam condensing on droplets at low temperatures within this range of Reynolds number. Yuen and Chen (Yuen and Chen, 1978) experiment measured the heat transfer rate of various liquid droplets (water and methanol) at higher temperatures, providing the data to develop and validate the extended correlations. Fig. 5 presents the comparisons between the experimental data and the correlations, which reveals that heat and mass transfer rates at high temperatures are lower than the predictions of the Ranz and Marshall correlation. The experimental data lie below the standard curve, indicating a reduction in evaporation heat transfer. The extended correlation with a correction factor of $(1 + B_T)^{-2/3}$ seems to yield better results in the high temperature range from 200 °C to 1000 °C. Previous authors commented on the reduction in heat transfer by adjusting the exponent of $(1+B_T)$ (Yuen and Chen, 1978). It is notable that the temperature range is so wide that the extended correlation is suitable for nuclear severe accident conditions, even for spray droplet evaporation under a hydrogen fire. However, when the droplet is heated up to the boiling temperature by the superheated gas, a boiling rate equation in the heat transfer model should be applied using a modified $B_T = \frac{c_{p,\infty}(T_\infty - T_p)}{L_{fg}}$.

The aforementioned analysis of the CARAIDAS experiments indicates that the Ranz and Marshall correlation underpredicts the evaporation rate, as seen in Fig. 3, for cases EVAP18 and EVAP21, for instance. The gas temperature (100–135 °C) in these cases is relatively higher than in

Table 2
Gas characteristics and droplet initial conditions (Malet et al., 2011).

Test	Pressure, Bar	Temperature, °C	Relative humidity, %	Droplet temperature, °C	Droplet diameter, μm	Droplet velocity, m/s
EVAP3	1.00	20.1	20.5	20.6	611 ± 4	3.58
EVAP13	5.42	100.1	15.0	31.0	605 ± 4	3.75
EVAP18	1.00	135.2	3.0	30.9	309 ± 5	3.66
EVAP21	4.29	97.4	12.0	29.2	311 ± 7	3.63
EVAP24	4.97	135.0	4.0	30.3	296 ± 4	3.10
COND1	4.00	141.3	55.0	36.0	341 ± 2	4.90
COND2	4.80	141.6	71.0	37.0	344 ± 2	4.70
COND7	5.30	139.3	87.0	35.0	593 ± 11	2.10
COND10	2.40	121.5	79.0	16.0	673 ± 5	2.10

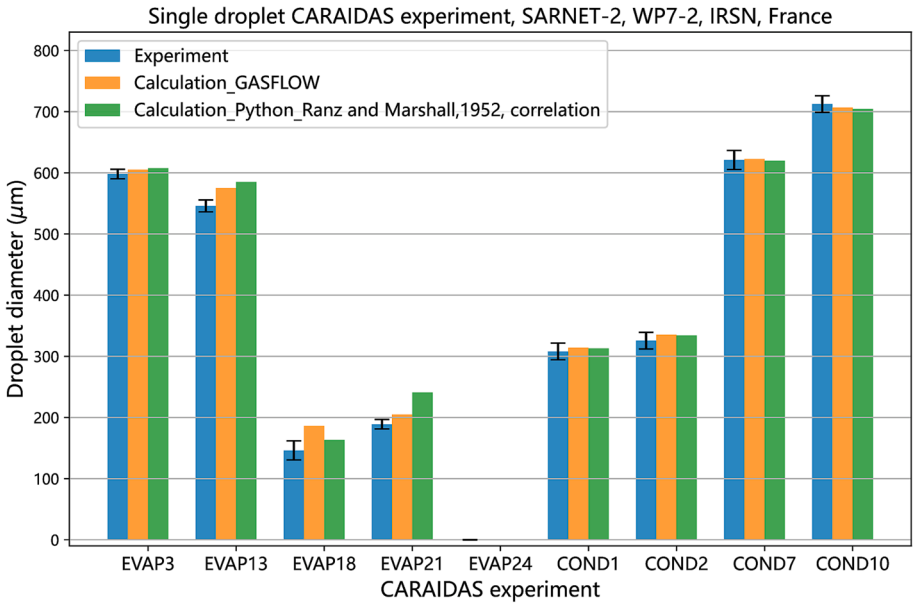

Fig. 3. Droplet diameter comparison between predictions and experimental data, Z 4.39 m (Interval of confidence 67%).

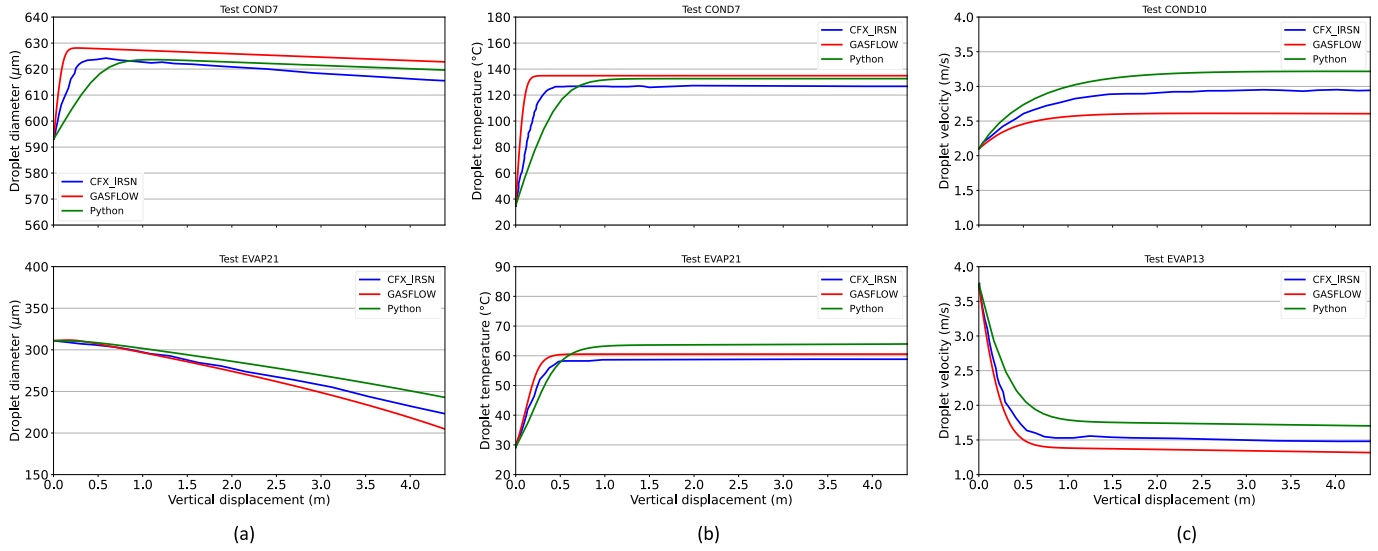

Fig. 4. Droplet diameter, temperature, and velocity along the height.

other cases. The evaporation rate could reduce since the vapor concentration at the surface is a balance of production on one hand and diffusion and convection on the other hand. It is certain that the expectation by using the extended correlation would be worse in these cases. We comment here that the uncertainties of the evaporation tests could play an important role in the discrepancy. Uncertainties of the tests with both condensation and evaporation are difficult to observe because the discrepancy of condensation is compensated by that of evaporation, vice versa. A bias of the case EVAP24 with various correlations is expected since the droplet size reduces a lot, and the time-accumulated bias would appear clearly.

Fig. 6 shows the calculated results of EVAP24 by our Python script with the two heat and mass transfer correlations. The "high" temperature in the legend means the gas temperature of 270 °C (double that of 135), the "middle" temperature is exactly the test temperature of 135 °C, and the "low" temperature donates 67.5 °C (half of 135 °C) for comparison. The other parameters are the same as those of EVAP24 test conditions, as seen in Table 2. We can see that, at the beginning, the temperature of the droplet rises rapidly when the droplet is suddenly exposed to the hot environment. Evaporation affects heat transfer rates through the changes in both the composition (non-condensable gas) and temperature of the surrounding gaseous medium. For the low gas temperature, this effect is weak (Nu*/Nu = ~0.98) and has almost no influence on the developments of droplet temperature, velocity, and diameter (until becoming a very tiny size). On the contrary, for the high gas temperature, the bias of these predictions with the two correlations is pronounced (Nu*/Nu = ~0.7), as well as for the middle gas temperature (Nu*/Nu = ~0.84). Droplet temperature predicted by the extended correlation is lower because of the reduction of Nu; as a result, the diameter is larger, as well as the mass-dependent velocity. The deviation of droplet temperature keeps almost stable, but those of the velocity and diameter increase over time due to the accumulation of deviation. The higher the gas temperature, the more significant its effect on heat transfer.

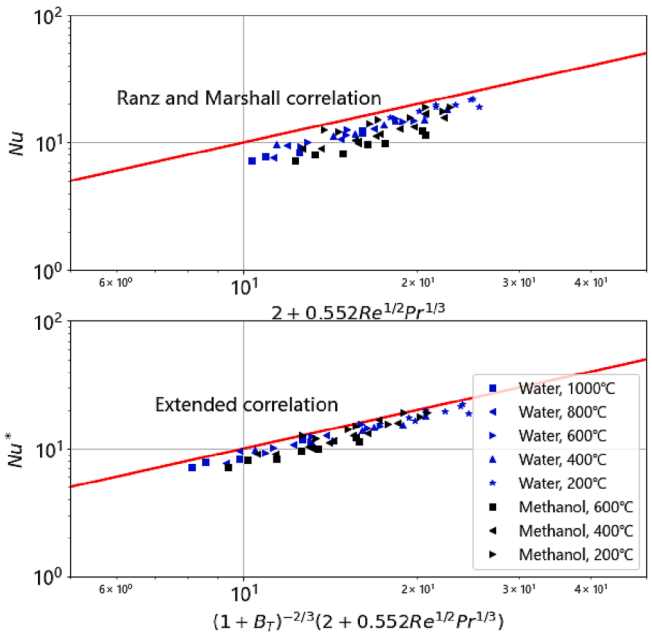

Fig. 5. Validation of droplet heat transfer correlations.

4.2. *Effects of curvature and solute*

The effects of curvature and solute are discussed together, as these two effects are pronounced only for small droplets. We analyzed the curvature and solute effects on small droplet evaporation and condensation using the test conditions of EVAP24. We assumed that CsI particles with a diameter of 100 nm dissolve in the evaporating water droplet, as well as in the hygroscopic growth of the aerosol particle. This size is typically used for the initial size of aerosol hygroscopic growth under severe accidents (Li et al., 2020; Mishra et al., 2019). To investigate the curvature effect, we let the droplet evaporate starting at an initial diameter of 1 μm (instead of the initial test diameter of 296 μm). The other thermal conditions are the same as those in the EVAP24 test. The calculation results of this evaporating droplet in 4% dry air with a relative humidity (RH) of 100% are shown in the upper subfigure of Fig. 7. The droplet diameter varies similarly for the cases with and without the curvature effect until the droplet diameter is very small (<0.1 μm). When the solute effect is considered, the droplet would evaporate until reaching an equilibrium diameter. We can see that the curvature effect governs the increase of evaporation, while the solute effect decreases the evaporation. Moreover, the solute effect causes the droplet to approach a final stable diameter since the increasing solute concentration decreases the vapor pressure over the solution droplet. When the vapor pressure balances with the relative humidity of the atmosphere, the equilibrium diameter appears. In this case, it is 0.106 μm, slightly larger than the dry CsI aerosol diameter of 0.1 μm. This

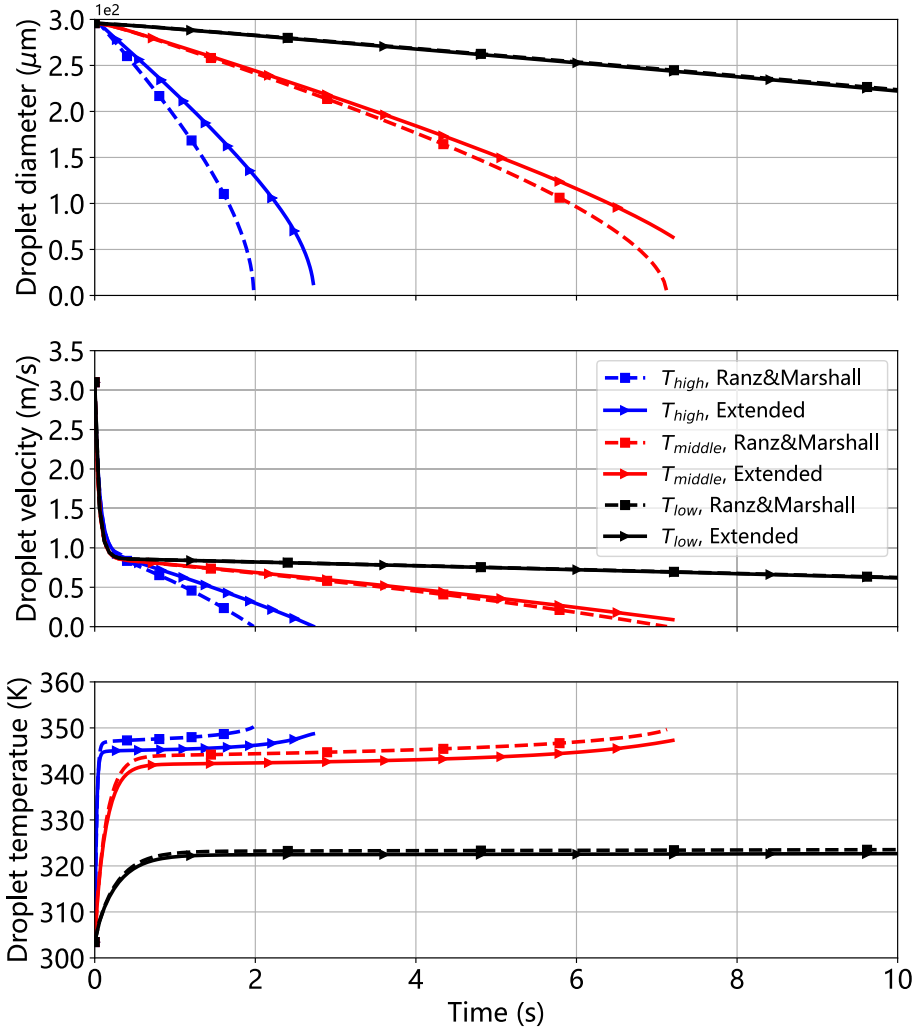

Fig. 6. Development of droplet diameter, velocity, and temperature (CARAIDAaraidas EVAP24 Test).

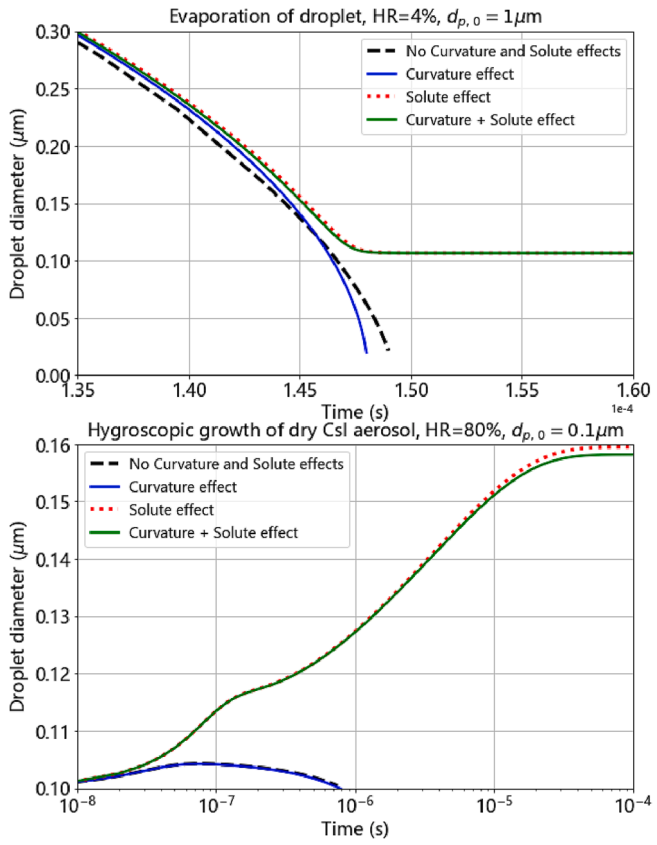

Fig. 7. Curvature and solute effects in droplet evaporation and condensation.

equilibrium diameter mainly depends on the relative humidity and the solute mass dissolved in the water droplet.

To investigate the effect of solutes on the hygroscopic growth of aerosols, we allowed particles to condense from an initial dry diameter of 0.1 μm CsI, and changed the relative humidity to 80%. The other thermal conditions were identical to those of the EVAP24 test. The predicted results of this droplet hygroscopic growth are presented in the lower subfigure of Fig. 7. The curves without solute effect show, at the very beginning, a tiny increase in diameter due to the condensation driven by the temperature difference. The droplet evaporates to a dry diameter once the droplet temperature is close to the gas temperature. The observed droplet dynamics are quite different if the solute effect is considered. The droplet diameter increases until it reaches an equilibrium value of 0.16 μm, which is quite larger than the evaporating case of 0.106 μm, just due to the higher relative humidity. The curvature effect is negative, but the solute effect dominates the aerosol growth. The growth factors (ratio of equilibrium diameter to the dry aerosol diameter) are 1.06 for HR 4% and 1.6 for HR 80% for CsI aerosol in a containment atmosphere, which is consistent with the experimental data in Ref. (Mishra et al., 2019).

The small droplet evaporation and aerosol growth are completed in a very short time, so in nuclear engineering field, the temperature gradient between droplet and gas is often ignored to simplify the process as a quasi-steady state. Therefore, when simulating the spray droplets in a containment atmosphere, the minimum droplet size can be truncated as small as the equilibrium diameter in the evaporation case, and the droplet size can be initialized as large as the hygroscopic growth in the condensation case.

5. Conclusions

The spray system prevents overpressure in nuclear containment in case of steam injection. It also aims to enhance gas mixing in the presence of hydrogen and wash-out airborne radioactive aerosols. Spray droplets could evaporate under high gas temperatures (>200 °C) and with the effect of the dissolved aerosols CsI and CsHO. The droplet heat transfer model with respect to the above conditions is extended and coupled in a Lagrangian droplet-tracking approach. Conclusions are obtained as follows:

1. The behavior of a single droplet reveals good agreement in the comparisons between the newly developed approach and the experimental data. However, there are still uncertainties in droplet evaporation, as seen in simulations of CARAIDAS evaporation tests.
2. High gas temperatures reduce heat transfer rates by a factor of $(1 + B_T)^{2/3}$. The bias of the predictions with/without the high gas temperature effect is pronounced (Nu*/Nu = 0.7–0.84). The droplet diameter predicted by the extended model is larger than the original one because of the reduction of Nu. The higher the gas temperature, the greater the reduction of droplet evaporation.
3. Droplet curvature enhances droplet evaporation, but this effect only works for tiny droplets (<100 nm). Solute effect is essential for small droplet evaporation and dry aerosol growth, which dominate the final equilibrium droplet diameter. The droplet equilibrium diameter mainly depends on the relative humidity and the solute mass dissolved in the water droplet. However, it is recommended to investigate further the impact of reducing solute molar concentration in the droplet on aerosol hygroscopic growth.
4. The extended droplet/aerosol heat transfer model considers new features, which fill the gap in knowledge of the containment spray under severe accidents. This approach is valuable not only for improving the accuracy of the spray model but also for simplifying the minimum spray droplet size as a truncated or initialized equilibrium diameter in containment codes for applications.

Spray swarms can significantly mix gas. Simulations (Wang et al., 2023) of the TOSQAN test 113 and test 101 spray experiments have been completed to investigate the two-way coupling phenomena in the containment atmosphere, including spray entrainment, gas mixing, and thermal dynamics such as droplet swarm cooling of the containment, the effect of spray shape, droplet size, and the evaporation of the spray-formed film on containment walls, and so on.

CRediT authorship contribution statement

Fangnian Wang: Conceptualization, Writing – original draft. **Jianjun Xiao:** Software, Writing – review & editing. **Thomas Jordan:** Supervision, Project administration.

Declaration of Competing Interest

The authors declare that they have no known competing financial interests or personal relationships that could have appeared to influence the work reported in this paper.

Data availability

The authors do not have permission to share data.

Acknowledgements

This work is supported by Innovations pool project 2021-2023 from Helmholtz-Forschungsbereich Energie – Programm MTET Zukunftsthema “Solarer Wasserstoff – hochrein und komprimiert”, Grant: 38.02.02, 38.04.03, 38.05.01

References

Abramzon, B., Sirignano, W.A., 1989. Droplet vaporization model for spray combustion calculations. Int. J. Heat Mass Transf. 32 (9), 1605–1618.

Amani, E., Nobari, M.R.H., 2013. A calibrated evaporation model for the numerical study of evaporation delay in liquid fuel sprays. Int. J. Heat Mass Transf. 56 (1–2), 45–58.

Babić, M., Kljenak, I., Mavko, B., 2009. Simulations of TOSQAN containment spray tests with combined Eulerian CFD and droplet-tracking modelling. Nucl. Eng. Des. 239 (4), 708–721.

Kevin Bowley, 2021. Fundamentals of Atmospheric Science. Lecture in Pennsylvania State University. https://www.e-education.psu.edu/meteo300/.

Clift, R., Grace, J.R., Weber, M.E., 1978. Bubbles, drops, and particles.

Crowe, C., Schwarzkopf, J., Sommerfeld, M. and Tsuji, Y., 2012. Multiphase Flows with droplets and particles, second edition.

Ding, P., Liu, Y., Wang, B., Li, W., Wang, J., 2017. The homogeneous and Lagrangian tracking approaches of the spray simulation in the containment. Ann. Nucl. Energy 101, 203–214.

Foissac, A., Malet, J., Vetrano, M.R., Buchlin, J.-M., Mimouni, S., Feuillebois, F., Simonin, O., 2011. Droplet size and velocity measurements at the outlet of a hollow cone spray nozzle. Atomization Sprays 21 (11), 893–905.

Foissac, A., Malet, J., Mimouni, S., Ruyer, P., Feuillebois, F., Simonin, O., 2013. Eulerian simulation of interacting PWR sprays including droplet collisions. Nucl. Technol. 181 (1), 133–143.

Foissac, A., 2011. Modelling the droplet interaction in a hostile environment (No. FRNC-TH–8626). Doctoral these, Universite de Paris VI.

Gunn, R., Kinzer, G.D., 1949. The terminal velocity of fall for water droplets in stagnant air. J. Atmospheric Sci. 6 (4), 243–248.

Gupta, S., Schmidt, E., Freitag, M., Langerock, G. and Funke, F., 2017, May. Experimental investigations on containment spray performance under severe accident conditions. In Proceedings of 8th European Review Meeting on Severe Accident Research (ERMSAR), Warsaw, Poland.

IAEA, 2011. Mitigation of Hydrogen Hazards in Severe Accidents in Nuclear Power Plants. IAEA TECDOC-1661, International Atomic Energy Agency, Vienna, p. 2011.

Köhler, H., 1936. The nucleus in and the growth of hygroscopic droplets. Trans. Faraday Soc. 32 (0), 1152–1161.

Kuerten, J.G.M., 2016. Point-Particle DNS and LES of particle-laden turbulent flow-a state-of-the-art review. Flow Turbul. Combust. 97 (3), 689–713.

Li, Y., Zhou, Y., Sun, Z., Gu, H., Ma, Q., Diao, H., 2020. Analysis of hygroscopic growth properties of soluble aerosol under severe nuclear accidents conditions. Prog. Nucl. Energy 127, 103464.

Malet, J., Blumenfeld, L., Arndt, S., Babic, M., Bentaib, A., Dabbene, F., Kostka, P., Mimouni, S., Movahed, M., Paci, S., Parduba, Z., Travis, J., Urbonavicius, E., 2011. Sprays in containment: final results of the SARNET spray benchmark. Nucl. Eng. Des. 241 (6), 2162–2171.

Malet, J., Gelain, T., Mimouni, S., Manzini, G., Arndt, S., Klein-Hessling, W., Xu, Z., Povilaitis, M., Kubisova, L., Parduba, Z. and Paci, S., 2011. Spray model validation on single droplet heat and mass transfers for containment applications-SARNET-2 benchmark. The 14th International Topical Meeting on Nuclear Reactor Thermalhydraulics, September 25-30th, 2011, Toronto, Canada.

Mimouni, S., Lamy, J.S., Lavieville, J., Guieu, S., Martin, M., 2010. Modelling of sprays in containment applications with a CMFD code. Nucl. Eng. Des. 240 (9), 2260–2270.

Mishra, G., Mandariya, A.K., Tripathi, S.N., Mariam, Joshi, M., Khan, A., Sapra, B.K., 2019. Hygroscopic growth of CsI and CsOH particles in context of nuclear reactor accident research. J. Aerosol Sci 132, 60–69.

OECD, 2012. OECD/SETH-2 project PANDA and MISTRA experiments final summary report. Investigation of key issues for the simulation of thermal-hydraulic conditions in water reactor containment. OCDE Report, France.

Oseen, C.W., 1910. Uber die Stokes' sche Formel und Uber eine verwandte Aufgabe in der Hydrodynamik. Arkiv Mat., Astron. och Fysik, 6, p.1.

Plumecocq, W., Passalacqua, R., 2001. Status of emergency spray modelling in the integral code ASTEC. Proceedings of the 9th international conference on nuclear engineering, ICONE-9, April 8-12, 2001, Palais des congres Acropolis, Nice, France.

Pruppacher, H.R., Klett, J.D., 1980. Microphysics of clouds and precipitation. Nature 284 (5751), 88.

Putnam, A., 1961. Integratable form of droplet drag coefficient. Ars Journal 31 (10), 1467–1468.

Rabe, C., Malet, J., Feuillebois, F., 2010. Experimental investigation of water droplet binary collisions and description of outcomes with a symmetric Weber number. Physics of fluids, 22(4), p.047101.

Ranz, W.E., Marshall, W.R., 1952. Evaporation from drops: Part I & II. Chem. Eng. Prog 48, 173–180.

Renksizbulut, M., Yuen, M.C., 1983. Experimental study of droplet evaporation in a high-temperature air stream. J. Heat Transfer 105 (2), 384–388.

Renksizbulut, M., Nafziger, R., Li, X., 1991. A mass transfer correlation for droplet evaporation in high-temperature flows. Chem. Eng. Sci. 46 (9), 2351–2358.

Schiller, L., Naumann, A., 1935. A drag coefficient correlation. Z. Ver. Dtsch. Ing. 1935 (77), 318–320.

Spalding, D.B., 1953. The combustion of liquid fuels. Symp. (Int.) Combust. 4 (1), 847–864.

Strizhak, P.A., Volkov, R.S., Castanet, G., Lemoine, F., Rybdylova, O., Sazhin, S.S., 2018. Heating and evaporation of suspended water droplets: experimental studies and modelling. Int. J. Heat Mass Transf. 127, 92–106.

Tinarelli, G., Mortarini, L., Castelli, S.T., Carlino, G., Moussafir, J., Olry, C., Armand, P., Anfossi, D., 2012. Review and validation of MicroSpray, a Lagrangian particle model of turbulent dispersion. Lagrangian Model. Atmosphere 200, 311–328.

Topping, D.O., McFiggans, G.B., Coe, H., 2005. A curved multi-component aerosol hygroscopicity model framework: Part 1–Inorganic compounds. Atmos. Chem. Phys. 5 (5), 1205–1222.

van Sebille, E., Griffies, S.M., Abernathey, R., Adams, T.P., Berloff, P., Biastoch, A., Blanke, B., Chassignet, E.P., Cheng, Y.u., Cotter, C.J., Deleersnijder, E., Döös, K., Drake, H.F., Drijfhout, S., Gary, S.F., Heemink, A.W., Kjellsson, J., Koszalka, I.M., Lange, M., Lique, C., MacGilchrist, G.A., Marsh, R., Mayorga Adame, C.G., McAdam, R., Nencioli, F., Paris, C.B., Piggott, M.D., Polton, J.A., Rühs, S., Shah, S.H. A.M., Thomas, M.D., Wang, J., Wolfram, P.J., Zanna, L., Zika, J.D., 2018. Lagrangian ocean analysis: Fundamentals and practices. Ocean Model. 121, 49–75.

Wang, F., Cheng, X.u., 2020. Extension and validation of aerosol wash-down model on inclined wall. Ann. Nucl. Energy 144, 107506.

Wang, F., Cheng, X.u., Gupta, S., 2021. COCOSYS analysis on aerosol wash-down of THAI-AW3 experiment and generic containment. Ann. Nucl. Energy 153, 108076.

Wang, F., Xiao, J., Jordan, T., 2023. Two-way Eulerian-Lagrangian coupling approach in GASFLOW code for containment spray modelling. Nucl. Eng. Des. 413, 112495.

Whang, S., Park, H.S., Kim, J., 2021. In-depth analysis of mixing characteristics of stratified gases during spray operation in the TOSQAN Test 113 using OpenFOAM. Nucl. Eng. Des. 373, 111012.

Wu, Z., Cao, Y., 2015. Numerical simulation of flow over an airfoil in heavy rain via a two-way coupled Eulerian-Lagrangian approach. Int. J. Multiph. Flow 69, 81–92. Xiao, J., Svishchev, A., Jordan, T., 2013, July. Development and Validation of Two-Way Fluid-Particle Coupling in Turbulent Flows for a CFD Code. In International Conference on Nuclear Engineering (Vol. 55805, p. V003T10A005). American Society of Mechanical Engineers.

Yuen, M.C., Chen, L.W., 1976. On drag of evaporating liquid droplets. Combust. Sci. Technol. 14 (4–6), 147–154.

Yuen, M.C., Chen, L.W., 1978. Heat-transfer measurements of evaporating liquid droplets. Int. J. Heat Mass Transf. 21 (5), 537–542.

Zhifu, Z., Guoxiang, W., Bin, C., Liejin, G., Yueshe, W., 2013. Evaluation of evaporation models for single moving droplet with a high evaporation rate. Powder Technol. 240, 95–102.